Science Advances
AAAS

advances.sciencemag.org/cgi/content/full/5/8/eaau9956/DC1

Supplementary Materials for

Ultrafast nonlocal collective dynamics of Kane plasmon-polaritons in a narrow-gap semiconductor

A. Charnukha*, A. Sternbach, H. T. Stinson, R. Schlereth, C. Brüne, L. W. Molenkamp, D. N. Basov

*Corresponding author. Email: a.charnukha@ifw-dresden.de

Published 9 August 2019, *Sci. Adv.* **5**, eaau9956 (2019)
DOI: 10.1126/sciadv.aau9956

This PDF file includes:

Section S1. Sample characterization

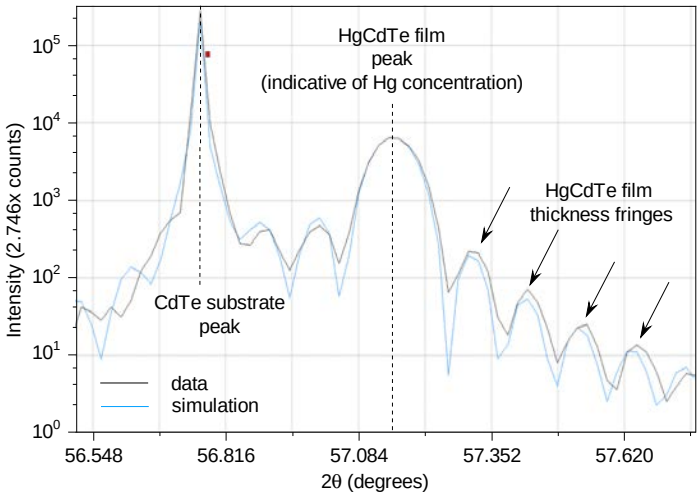

Fig. S1. Sample characterization. X-ray-diffraction intensity as a function of diffraction angle obtained on the HgCdTe thin film used in the experiments described in the main text (black line). Simulated trace fitted to the experimental data (blue line) with the Hg concentration (81% and thin-film thickness (90nm) extracted as best fit parameters.

Section S2. Photoinduced near-field optical response

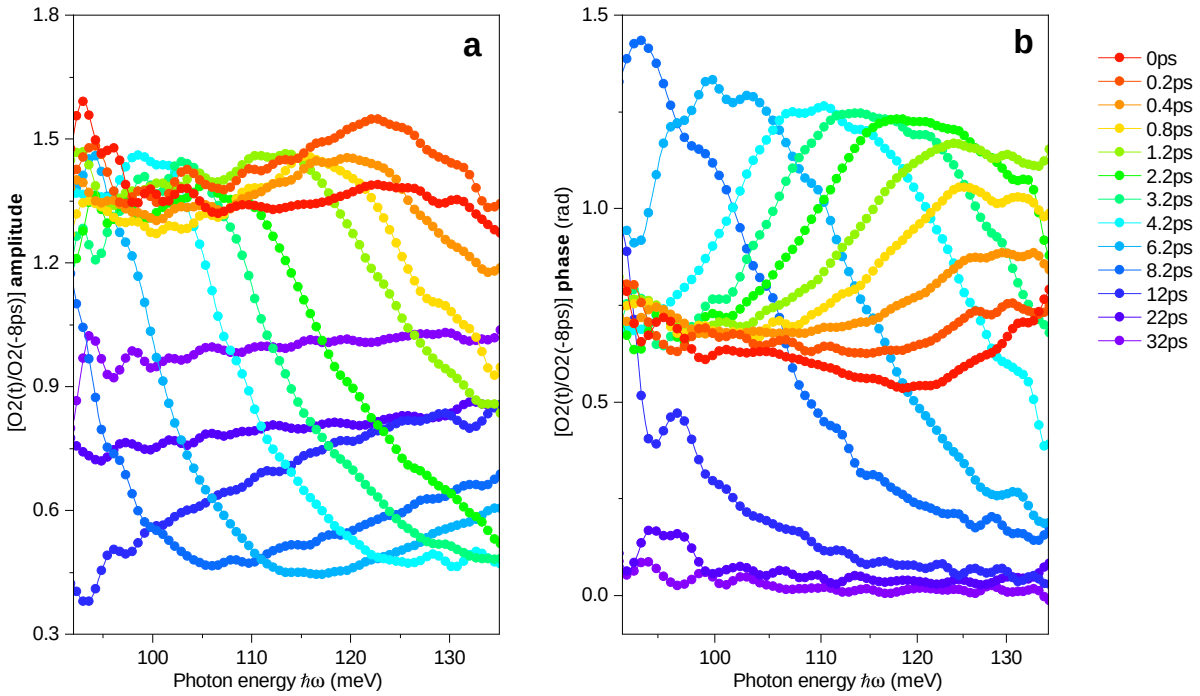

Fig. S2. Photoinduced near-field optical response. (Same data as in Figs.1b,c, displayed as a two-dimensional plot.) Photon-energy dependence of the amplitude **a** and phase **b** of the normalized transient near-field signal demodulated at the second harmonic of the tip tapping frequency. The spectra are plotted for various pump-probe delays from 0 ps to 12.2 ps and a pump pulse energy of 1 nJ.

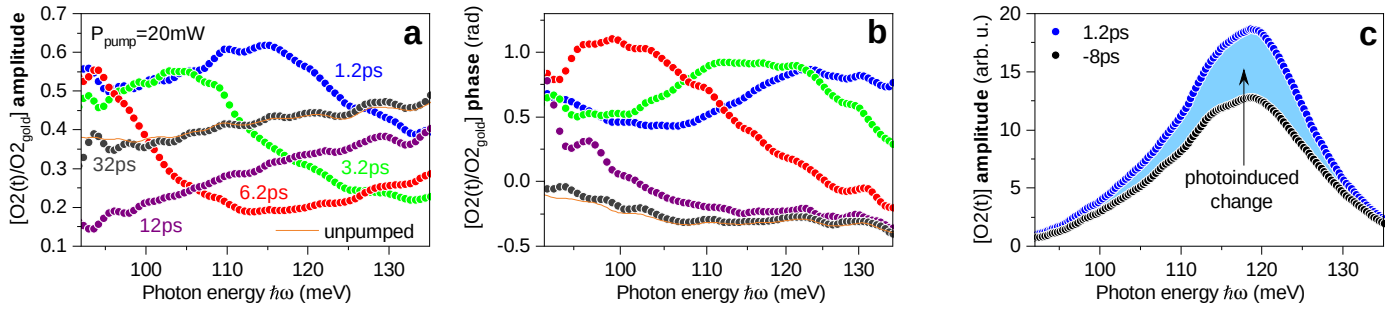

Fig. S3. Reference measurements and unnormalized spectra. Photon-energy dependence of the amplitude **a** and phase **b** of the transient near-field signal demodulated at the second harmonic of the tip tapping frequency as shown in Figs.1b,c of the main text but normalized to the corresponding reference signal obtained on gold rather than to that of the sample before the arrival of the pump pulse. Note the smaller relative magnitude of the near-field amplitude and phase due to the significantly stronger near-field response of metallic gold than semiconducting $Hg_{0.81}Cd_{0.19}Te$. **c**, Photon-energy dependence of the amplitude of the unnormalized transient near-field signal demodulated at the second harmonic of the tip tapping frequency, obtained 1.2 ps after (blue symbols) and 8 ps before (black symbols) the arrival of the pump pulse. Shaded area indicates the photoinduced change in the sample's near-field response.

Section S3. Reflection coefficient $r_p(\omega, q)$

The large-momentum reflection coefficient $r_p(\omega,q)$ (with q well beyond the light cone) of thin-film $Hg_{0.81}Cd_{0.19}Te$ on CdTe substrate was calculated using the standard expression for the combined reflection from two interfaces (air–$Hg_{0.81}Cd_{0.19}Te$ and $Hg_{0.81}Cd_{0.19}Te$–substrate; reflection from the bottom surface of the substrate has been neglected)

$$r_{p,total}(\omega,q,d_{\rm film}) = \frac{r_{p,{\rm air-film}}(\omega,q)+r_{p,{\rm film-sub}}(\omega,q)\exp[i2k_{z,{\rm film}}(\omega,q)d_{\rm film}]}{1+r_{p,{\rm air-film}}(\omega,q)r_{p,{\rm film-sub}}(\omega,q)\exp[i2k_{z,{\rm film}}(\omega,q)d_{\rm film}]} \quad \text{(S1)}$$

$$r_{p,{\rm air-film}}(\omega,q) = \frac{\varepsilon_{{\rm film},ab}(\omega)\,k_{z,{\rm air}}(\omega,q)-\varepsilon_{\rm air}(\omega)\,k_{z,{\rm film}}(\omega,q)}{\varepsilon_{{\rm film},ab}(\omega)\,k_{z,{\rm air}}(\omega,q)+\varepsilon_{\rm air}(\omega)\,k_{z,{\rm film}}(\omega,q)} \quad \text{(S2)}$$

$$r_{p,{\rm film-sub}}(\omega,q) = \frac{\varepsilon_{\rm sub}(\omega)\,k_{z,{\rm film}}(\omega,q)-\varepsilon_{{\rm film},ab}(\omega)\,k_{z,{\rm sub}}(\omega,q)}{\varepsilon_{\rm sub}(\omega)\,k_{z,{\rm film}}(\omega,q)+\varepsilon_{{\rm film},ab}(\omega)\,k_{z,{\rm sub}}(\omega,q)} \quad \text{(S3)}$$

$$k_{z,mat}(\omega,q) = \sqrt{\varepsilon_{mat}(\omega)\times(\omega/c)^2-q^2},\ mat={\rm film},ab;{\rm sub};{\rm air} \quad \text{(S4)}$$

In the above expressions $r_{p,if}$ denotes the Fresnel reflection coefficient for p-polarized light (along the AFM tip shaft in our experiments) for a given interface if (air-film and film-substrate), $\varepsilon_{mat}(\omega)$ is the frequency-dependent complex dielectric function of material mat (air, film, substrate), $k_{z,mat}(\omega,q)$ is the z-component of the photon momentum at frequency ω, q is the in-plane photon momentum (transferred to excited quasiparticles), ω/c is the total photon momentum, c is the speed of light, and $d_{\rm film}$ is the thickness of the $Hg_{0.81}Cd_{0.19}Te$ thin film.

In the mid-infrared spectral range of interest (80-140 meV) and in the absence of intrinsic of extrinsic charge carriers, the optical constants of both the $Hg_{0.81}Cd_{0.19}Te$ thin film and CdTe substrate can be determined using the following equation (Ref. 8): $\varepsilon_\infty = 15.2-15.6x+8.2x^2$, where x is the Cd content. This empirical dependence was established for bulk materials; epitaxially grown thin films are expected to experience substrate-induced strain (which can be estimated to about 0.2–0.3% in our material). Strain-induced change in the optical constants is significantly smaller than the difference in the optical constants of $Hg_{0.81}Cd_{0.19}Te$ and CdTe and can be neglected to first order. CdTe has a band gap (1.65 eV) significantly larger than the photon energy of our probe beam and does not show intrinsic doping. Therefore, its optical response in the mid-infrared spectral range can be well described by a single real constant $\varepsilon_{\rm sub}(\omega)=\varepsilon_{{\rm sub},\infty}$. The response of the $Hg_{0.81}Cd_{0.19}Te$ thin film consists of the real constant $\varepsilon_{{\rm film},\infty}$, itinerant response of (relatively low-concentration) intrinsic and (high-concentration) photoinduced charge carriers, as described in detail in the main text. Additionally, given that the band gap of $Hg_{0.81}Cd_{0.19}Te$ falls into the investigated spectral range, interband absorption is expected to contribute to $\varepsilon_{{\rm film},ab}(\omega)$. This contribution has a weak signature in the reflection coefficient, in stark contrast to the transmission/absorption coefficient, and was likewise neglected to minimize the number of fit parameters in our quantitative fits. Introduction of a band edge into the fits has been confirmed to have no substantial change on the results.

The computed reflection coefficient $r_p(\omega,q)$ of $Hg_{0.81}Cd_{0.19}Te$/CdTe using the material parameters described above is shown in Fig.2b for representative value of unscreened photoinduced plasma frequency $\omega_{\rm pl}=440$ meV and charge-carrier scattering rate $\gamma=12$ meV (to make quasiparticle dispersions more distinct). Figure S4a demonstrates the effect of varying the thin-film thickness on the reflection coefficient obtained in this model, while keeping all other material parameters constant (with the exception of a reduced value of the charge-carrier scattering rate $\gamma=1.2$ meV chosen to make the quasiparticle dispersions more distinct). Thinner

films give rise to larger slope in the plasmon-polariton dispersion of the low-energy branch (larger group velocity of propagating excitations) but, at the same time, lower characteristic energy. The latter implies that higher pump fluences are required to push the photoinduced plasmon-polariton frequency into the experimentally accessible spectral range (80–140 meV). This latter observation dictated the original choice of the film thickness for our experiments using high-repetition-rate ultrafast laser system, in which the maximum pump fluency is predominantly limited by the tip-damage threshold due to heating. Figure S4b shows the reflection coefficient of a 1000-nm metallic film with the same unscreened plasma frequency as in fig. S4 but with $\varepsilon_\infty = 1$ and suspended in air (no substrate). The data are displayed at intermediate in-plane momenta q to demonstrate the acoustic and optical character of the two plasmon-polaritonic modes identified in the main text. The dark red triangular region emanating from the origin is the light cone of free-space electromagnetic radiation.

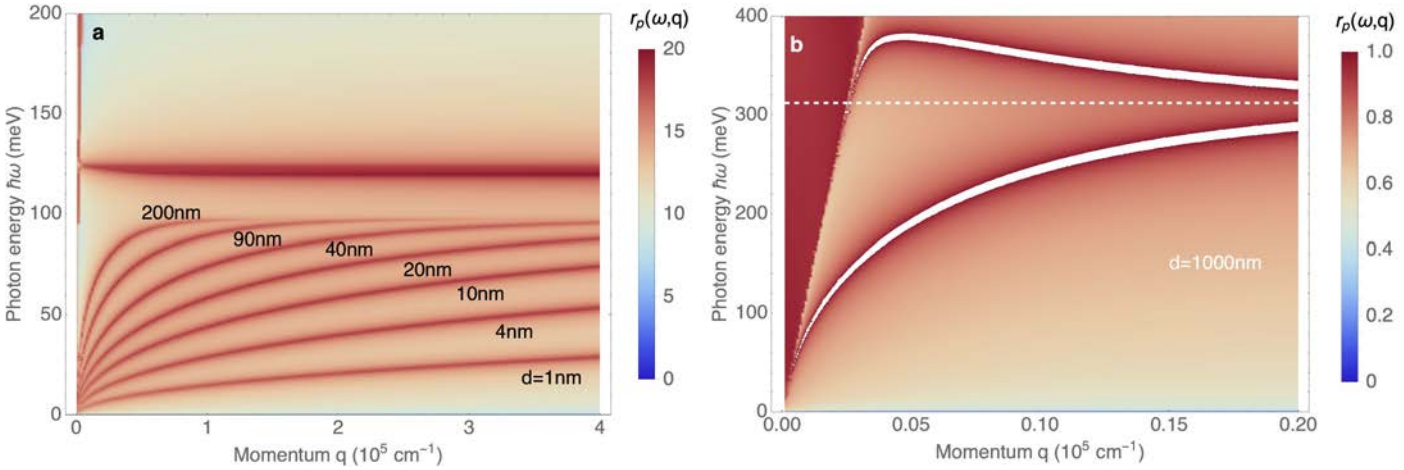

Fig. S4. Large-momentum plasmonic modes in $Hg_{0.81}Cd_{0.19}Te$/CdTe. a, Calculated photon-energy and momentum dependence of the Fresnel reflection coefficient $r_p(\omega, q)$ of an $Hg_{0.81}Cd_{0.19}Te$ thin film on CdTe substrate for various thin-film thicknesses. The calculation is identical to that in Fig.2b of the main text with the exception of the 10 times smaller quasiparticle scattering rate chosen to make the quasiparticle dispersions more distinct. **b**, Same as in panel **a** but for a fixed film thickness of 1000 nm, suspended in air (no substrate), and with $\varepsilon_\infty = 1$ to make the acoustic and optical character of the plamson-polaritonic dispersions in the long-wavelength limit apparent in our model. Note the significantly smaller scale of the quasiparticle momenta in this panel compared with panel **a** and Fig.2b. White dashed line indicates the energy of the surface plasmon-polariton (440 meV/$\sqrt{2}$), which both modes approach asymptotically at large momenta.

Section S4. Simulated far-field optical response

Near-field optical microscopy and spectroscopy provide access to large-momentum quasiparticle modes in a material, in stark contrast to conventional far-field spectroscopy, which only has access to the material response within the light cone, unless complex material patterning is implemented to induce large in-plane momentum transfer (e.g. via a diffraction grating). While the dynamics of both the plasma edge in far-field measurements and that of plasmon-polaritonic modes in near-field measurements is determined largely by the plasma frequency and the quasiparticle relaxation rate of the photoexcited particle-hole pairs, near-field spectroscopy is more sensitive to the optical response of thin and ultrathin films due to the much smaller penetration depth of near fields into the material than that of far fields, as shown in fig. S5. Figure S6 illustrates this point by displaying the calculated far-field reflectance of both bulk and thin-film $Hg_{0.81}Cd_{0.19}Te$ on CdTe using the same material parameters as those used in the fits of the near-field spectroscopy data for different values of photoinduced plasma frequency (figs. S6a,b) and for different thin-film thicknesses at one photoinduced plasma frequency (same as in Fig.2b and fig. S4). One can see that while the bulk response of $Hg_{0.81}Cd_{0.19}Te$ shows a shift of the photoinduced plasma edge analogous to the near-field results in the main text, that of the 90-nm thin film does not display a distinct feature at the plasma edge. The bulk behavior is largely recovered for 10-μm-thick $Hg_{0.81}Cd_{0.19}Te$/CdTe, as shown in fig. S6c. The steady-state plasma frequency in figs. S6b,c is taken as the intrinsic plasma frequency in the $Hg_{0.81}Cd_{0.19}Te$/CdTe sample investigated in our experiments (unscreened plasma frequency of 86 meV).

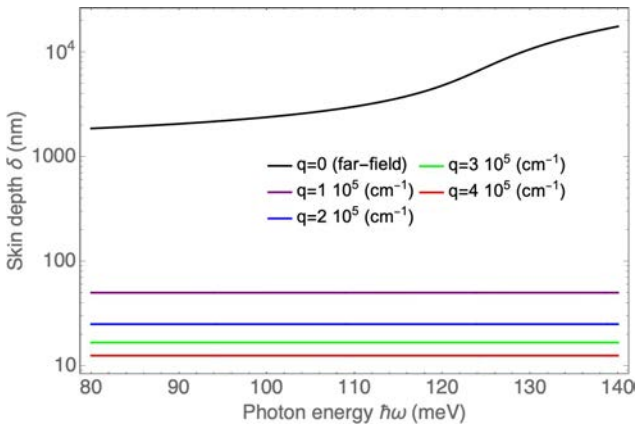

Fig. S5. Skin depth in bulk $Hg_{0.81}Cd_{0.19}Te$. Photon-energy dependence of the skin depth δ ($\delta^{-1} = 2\Im[k_{z,\mathrm{film}}(\omega,q)]$) of normal-incidence far-field ($q = 0$, black line) and large-momentum near-field electromagnetic radiation in bulk $Hg_{0.81}Cd_{0.19}Te$. Skin depth of near-field light is shown for four representative values of in-plane momentum q.

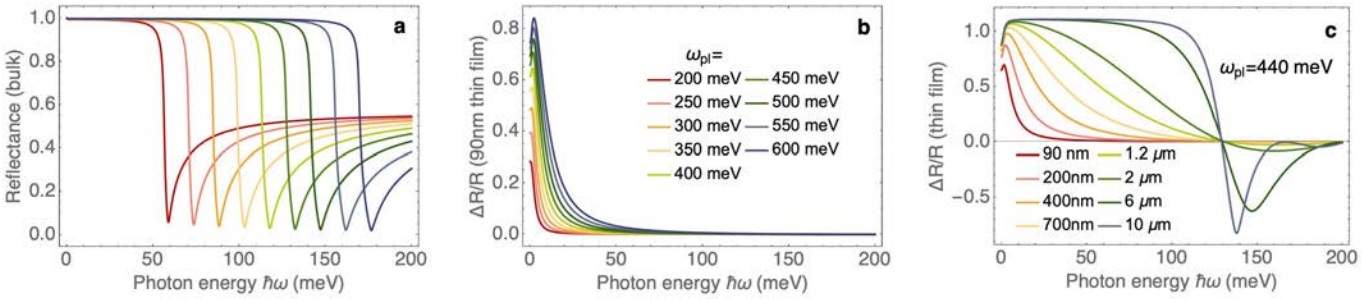

Fig. S6. Calculated far-field IR response. a,b, Calculated photon-energy dependence of the far-field reflectance of a *bulk* (**a**) and relative far-field reflectance change of a 90nm-thin-film (**b**) $Hg_{0.81}Cd_{0.19}Te$ material upon photoexcitation as a function of photoinduced plasma frequency, as indicated in the legend of panel **b**. While the calculated bulk far-field reflectance signal shows a clear plasma edge that shifts with increasing plasma frequency of photoexcited charge carriers, similarly to the main near-field plasmonic mode in Figs.1b,c, that of the thin film does not exhibit a clear far-field plasma edge or mode and only experiences a general background variation. Near-field signal, on the other hand, is dramatically more sensitive to plasmonic modes, as shown in Figs.1b,c and Fig.2c. **c**, Calculated photon-energy dependence of the relative far-field reflectance change upon photoexcitation of a thin-film of $Hg_{0.81}Cd_{0.19}Te$ of varying film thicknesses as indicated in the panel. The gradual transition from a low-frequency upturn to a clear reflectance edge is evident with increasing thin-film thickness.